Exploiting hidden symmetries to accelerate the lattice calculation of $K \to \pi\pi$ decays with G-parity boundary condititons

Christopher Kelly[a,*]

[a]*Computational Science Initiative,*
Brookhaven National Laboratory,
Upton, NY 11973, USA.

E-mail: ckelly@bnl.gov

The RBC & UKQCD collaborations have successfully employed G-parity boundary conditions in the measurement of $K \to \pi\pi$ decays to obtain a physical decay with the two-pion ground state, at the cost of a significant increase in computational expense. We report on new theoretical/algorithmic developments based upon the properties of the Dirac operator under complex conjugation that have been exploited to achieve highly significant computational cost reductions, and explain their impact on our ongoing effort to repeat the calculation on finer lattices.

The 40th International Symposium on Lattice Field Theory (Lattice 2023)
July 31st - August 4th, 2023
Fermi National Accelerator Laboratory

---

*Speaker

1. Introduction

Direct CP-violation (CPV) in $K \rightarrow \pi\pi$ decays was first measured in the late 1990s and early 2000s in a series of pioneering experiments at CERN and FermiLab, resulting in a determination for its measure, ϵ', with a 10% total error. This quantity is highly sensitive to new sources of CPV that may help explain the dominance of matter over antimatter in the observable Universe. As these decays receive large contributions from non-perturbative multi-particle hadronic physics, it was 2015 before the first *ab initio* Standard Model calculation was performed via lattice methods by the RBC & UKQCD collaborations [1], followed in 2020 by an updated result with much larger statistics and significantly improved control over systematic effects [2].

The lattice calculation involves measuring the three-point amplitudes $A_I = \langle (\pi\pi)_I | H_W | K^0 \rangle$ for isospin $I = 0$ and $I = 2$ two-pion states, where H_W is the weak effective Hamiltonian. In order to avoid potentially large charm discretization errors, the calculations have thus far been performed in the 3-flavor weak effective theory, for which

$$H_W = \sum_{i=1}^{10} c_i(\mu) Q_i(\mu), \tag{1}$$

where Q_i are effective four-quark operators and c_i are the Wilson coefficients that describe the high-energy physics, including that of the charm quark. Both components must be matched to the same renormalization scheme. ϵ' can be obtained directly from A_0 and A_2 via

$$\epsilon' = \alpha \frac{\text{Re}(A_2)}{\text{Re}(A_0)} \left(\frac{\text{Im}(A_2)}{\text{Re}(A_2)} - \frac{\text{Im}(A_0)}{\text{Re}(A_0)} \right), \tag{2}$$

where α comprises several other factors including the Lellouch-Lüscher finite-volume correction.

The 2015 and 2020 lattice calculations of the more-challenging $I = 0$ amplitude employed G-parity spatial boundary conditions (BCs) to remove the dominant contribution to the signal associated with the unphysical, energy non-conserving decay of a kaon to two pions at rest. This technique relies upon the fact that the pion states have G-parity eigenvalue -1, hence when imposed as a boundary condition the pion propagators perforce obey antiperiodic BCs and therefore have momenta that are odd-integer multiples of π/L (if non-interacting), where L is the lattice size. The at-rest pion state is thereby not an allowed finite-volume state, and the energy of the ground-state – comprising two pions moving back-to-back – can be tuned to match the kaon mass by adjusting the lattice size, thus ensuring the physical decay dominates the signal. This is achieved while preserving the vital isospin symmetry. However, it comes with the price of doubling the raw floating-point cost of applying the Dirac operator (cf. below) and requires the generation of custom gauge ensembles with these novel BCs. More recently we have begun exploring [3] the use of conventional, periodic BCs, which avoid these challenges at the cost of making the desired signal a subdominant, excited-state contribution. This includes avoiding the need for generating new ensembles, although we stress that this is only the case if one of the lower (preferably the first) excited finite-volume $\pi\pi$ states of the target existing ensemble has an energy close to or matching that of the kaon; if this is not the case, a custom ensemble with an appropriately tuned lattice size will be required regardless.

Our current best result [2] is $\text{Re}(\epsilon'/\epsilon)_{\text{lat}} = 21.7(2.6)_{\text{stat}}(8.0)_{\text{sys}} \times 10^{-4}$, where ϵ is the measure of indirect CPV. We observe good consistency with the experimental value $\text{Re}(\epsilon'/\epsilon)_{\text{expt}} = 16.6(2.3) \times 10^{-4}$, albeit with an error roughly $4\times$ larger and dominated by systematic effects. Given the potential for the discovery of a new physics, there is a strong motivation to reduce these errors. An estimated 12% systematic error comes from the Wilson coefficients, the calculation of which requires matching between the 3- and 4-flavor weak effective theories at the charm-mass scale, $m_c \sim 1.3$ GeV, where perturbation theory is less reliable. A larger, $\sim 23\%$ systematic error arises

from neglecting electromagnetic (EM) and isospin-breaking effects. Addressing these systematic errors will require significant computational resources and, for the latter, the development of appropriate techniques to control the finite-volume errors when including EM effects on the lattice. Progress by our collaborations on these fronts is reported in Refs. [4, 5]. A third, ~12% systematic error arises due to discretization effects from simulating A_0 with only a single, relatively coarse ($a^{-1} \approx 1.4$ GeV) lattice spacing. Addressing this error by repeating the calculation on one or more finer lattices and taking the continuum limit is much more readily achievable, and is the focus of our present activity. However, this is made challenging due to the expense of employing G-parity BCs. While adopting periodic BCs is an option, in this document we introduce new techniques that vastly reduce the cost of the G-parity calculation to the point where it regains its cost competitiveness.

2. G-parity BCs for quarks

Under G-parity the up and down quarks transform as $d \rightarrow C\bar{u}^T$, $u \rightarrow -C\bar{d}^T$ where C is the charge conjugation matrix. A convenient representation for implementation on the lattice is obtained by rewriting the theory in terms of the "flavor-doublet" fields [6]

$$\psi = \begin{pmatrix} d \\ C\bar{u}^T \end{pmatrix} \qquad \hat{G}\psi\hat{G}^{-1} = \begin{pmatrix} C\bar{u}^T \\ -d \end{pmatrix} = i\sigma_2\psi \qquad (3)$$

where $\hat{G}$ is the G-parity operator and σ_2 is the second Pauli matrix. In this form, the boundary operation becomes a simple transposition of column elements coupled with a sign. Gauge invariance requires that the gauge links obey charge-conjugation (complex-conjugation) BCs, which we incorporate by defining flavor-matrix gauge links

$$\tilde{U}_\mu = \begin{pmatrix} U_\mu & 0 \\ 0 & U_\mu^* \end{pmatrix}. \qquad (4)$$

The now two-flavor Dirac operator becomes

$$\mathcal{M}(x, y) = \sum_\mu \left[\tilde{U}_\mu(x)\Gamma_\mu^+ B_\mu^+(x_\mu)\delta_{x+\hat{\mu},y} + B_\mu^-(x_\mu)\tilde{U}_\mu^\dagger(y)\Gamma_\mu^-\delta_{x-\hat{\mu},y} \right] + m\delta_{x,y}. \qquad (5)$$

where $\Gamma^\pm = \frac{1}{2}(1 \mp \gamma^\mu)$ assuming Wilson-like fermions, $B_\mu^\pm$ are position-dependent flavor matrices that induce the flavor rotation at the boundary [6], and the light quarks are assumed (required to be) degenerate. By including the boundary operation explicitly here we can avoid ambiguity and treat all lattice coordinates as defined on a torus (i.e. modulo the lattice size), such that $x_\mu = L$ is equivalent to $x_\mu = 0$; $x_\mu = -1$ is equivalent to $x_\mu = L - 1$; etc.

The application of the two-flavor Dirac operator to a flavored field has twice the numerical cost as applying a single-flavor operator to an unflavored field. Thus, both measurements and ensemble generation are naturally twice as expensive as for an equivalent periodic BC calculation. A further complication arises from the fact that inversion of the Dirac operator through a conventional conjugate gradient algorithm requires squaring the operator to obtain a Hermitian, positive-definite matrix. This ties in to the calculation of the quark determinant through the pseudofermion method,

$$\det(\mathcal{M})^{2/n} = \int [d\phi_r][d\phi_i] \exp\left(-\phi^\dagger(\mathcal{M}\mathcal{M}^\dagger)^{-1/n}\phi\right), \qquad (6)$$

where the integral is performed explicitly over the real and imaginary parts, ϕ_r and ϕ_i, of the complex pseudofermion field ϕ. For 2 + 1f simulations with conventional BCs, this squaring is largely benign as $\det(\mathcal{M})^2$ represents the desired contribution of two degenerate light quark flavors, and an explicit square-root is required only for the cheaper, strange quark. However, for G-parity BCs, $\det(\mathcal{M})^2$ represents the contributions of *four* flavors and an explicit square- and fourth-root is required for the light and strange sectors, respectively. Our 2015 simulation [1] was performed

using the rational hybrid Monte Carlo (RHMC) approach for both light and strange quarks, whereby the n-th root is obtained via a rational approximation at significant additional computational cost. A later improvement incorporated TWQCD's "exact one-flavor" (EOFA) domain wall action [7, 8] in place of RHMC for the light sector, resulting in a 4.2× speed-up in ensemble generation [8], albeit still much slower than a calculation without G-parity BCs.

3. Subtle symmetries of the Dirac operator

In Ref. [6] we identified an interesting property relating $\mathcal{M}$ to its complex conjugate: We first define the real, anti-Hermitian spin matrix $X = C\gamma^5$, which relates the four space-time γ-matrices to their complex conjugates: $X^{-1}\gamma_\mu^* X = \gamma_\mu$. (Note also that $X^2 = -1$.) Likewise, σ_2 relates the flavor-matrix gauge links to their complex conjugates: $\sigma_2 \tilde{U}_\mu^* \sigma_2 = \tilde{U}_\mu$, and also commutes with the boundary operation σ_2 (present in the matrices $B_\mu^\pm$). Combining these into a Hermitian, unitary, involutory (self-inverse) spin-flavor matrix $\Xi = -i\sigma_2 X$ gives

$$\Xi^{-1}\mathcal{M}^*(x,y)\Xi = \mathcal{M}(x,y).\tag{7}$$

Complex conjugation of the Dirac operator is therefore equivalent to a unitary spin-flavor rotation. In Ref. [6] we exploited this property in a limited way to reduce the number of inversions when performing measurements with complex sources (e.g. momentum sources) for which both the inverse from the source and its complex conjugate are desired. However, a much more powerful use can be derived by examining the flavor structure implied by Eq. 7:

$$\mathcal{M} = \Xi^{-1}\mathcal{M}^*\Xi \tag{8a}$$

$$\begin{pmatrix} \mathcal{M}_{11} & \mathcal{M}_{12} \\ \mathcal{M}_{21} & \mathcal{M}_{22} \end{pmatrix} = \begin{pmatrix} X^{-1}\mathcal{M}_{22}^* X & -X^{-1}\mathcal{M}_{21}^* X \\ -X^{-1}\mathcal{M}_{12}^* X & X^{-1}\mathcal{M}_{11}^* X \end{pmatrix} \tag{8b}$$

$$\mathcal{M} = \begin{pmatrix} \mathcal{M}_{11} & \mathcal{M}_{12} \\ -X^{-1}\mathcal{M}_{12}^* X & X^{-1}\mathcal{M}_{11}^* X \end{pmatrix} \tag{8c}$$

where the last line is obtained by equating the lower rows. Introducing a rotation through a unitary matrix $R = \frac{1}{\sqrt{2}} \begin{pmatrix} -X & i \\ -1 & iX \end{pmatrix}$, related to Ξ by $\Xi = -RR^T$, gives

$$R^\dagger \mathcal{M} R = \begin{pmatrix} -\mathrm{Re}[X\mathcal{M}_{11}X + X\mathcal{M}_{12}] & -\mathrm{Im}[X\mathcal{M}_{11} + X\mathcal{M}_{12}X] \\ -\mathrm{Im}[\mathcal{M}_{11}X + \mathcal{M}_{12}] & \mathrm{Re}[\mathcal{M}_{11} + \mathcal{M}_{12}X] \end{pmatrix} \equiv \mathcal{M}_{\mathrm{re}}, \tag{9}$$

whose elements are all explicitly real. The G-parity Dirac operator can therefore be rotated into a pure-real matrix! An immediate application can be found in the pseudofermion integral, Eq. 6. Rewriting in terms of $\mathcal{M}_{\mathrm{re}}$ and $\phi' = R^\dagger \phi = \phi_r' + i\phi_i'$:

$$\det(\mathcal{M})^2 = \int [d\phi_r'][d\phi_i'] \exp\left(-\phi_r'^T (\mathcal{M}_{\mathrm{re}}\mathcal{M}_{\mathrm{re}}^T)^{-1}\phi_r' - \phi_i'^T (\mathcal{M}_{\mathrm{re}}\mathcal{M}_{\mathrm{re}}^T)^{-1}\phi_i'\right)$$
$$= \left[\int [d\phi_r'] \exp\left(-\phi_r'^T (\mathcal{M}_{\mathrm{re}}\mathcal{M}_{\mathrm{re}}^T)^{-1}\phi_r'\right)\right]^2 \tag{10a}$$

hence we circumvent the need for the square-root to obtain a two flavor determinant by evaluating the pseudofermion integral of $\mathcal{M}_{\mathrm{re}}$ with real, two-flavor pseudofermions:

$$\det(\mathcal{M}) = \int [d\phi_r'] \exp\left(-\phi_r'^T (\mathcal{M}_{\mathrm{re}}\mathcal{M}_{\mathrm{re}}^T)^{-1}\phi_r'\right). \tag{11}$$

Furthermore, applying a real matrix to a real vector requires less than half the floating-point operations than the equivalent complex operation, thus making its computational cost comparable to that of a single-flavor operator. Unfortunately, implementing $\mathcal{M}_{\mathrm{re}}$ such that this optimization is realized within an existing codebase such as Grid [9] is very challenging. Fortunately, we are able to rewrite this integral in a much more convenient form as we describe below.

4. X-conjugate Dirac operator

Taking the integrand of Eq. 11 and rewriting again in terms of $\mathcal{M}$,

$$-\phi_r'^T (\mathcal{M}_{\text{re}} \mathcal{M}_{\text{re}}^T)^{-1} \phi_r' = -\phi_r'^T R^\dagger (\mathcal{M}\mathcal{M}^\dagger)^{-1} R\phi_r' . \tag{12}$$

Defining $\chi \equiv R\phi_r'$ and writing in component form,

$$\chi = R \begin{pmatrix} \phi_{r,1}' \\ \phi_{r,2}' \end{pmatrix} = \frac{1}{\sqrt{2}} \begin{pmatrix} -X\phi_{r,1}' + i\phi_{r,2}' \\ -\phi_{r,1}' + iX\phi_{r,2}' \end{pmatrix} = \begin{pmatrix} \chi_1 \\ -X\chi_1^* \end{pmatrix}, \tag{13}$$

we observe that the real two-flavor pseudofermion fields ϕ_r' can be written in the original basis as complex two-flavor fields χ whose flavor components are related by complex conjugation and multiplication by X; we refer to these as "X-conjugate" vectors.

Applying $\mathcal{M}$ in the form Eq. 8c to an X-conjugate vector returns an X-conjugate vector:

$$\mathcal{M}\chi = \mathcal{M} \begin{pmatrix} \chi_1 \\ -X\chi_1^* \end{pmatrix} = \begin{pmatrix} \mathcal{M}_{11}\chi_1 - \mathcal{M}_{12}X\chi_1^* \\ -X[\mathcal{M}_{11}\chi_1 - \mathcal{M}_{12}X\chi_1^*]^* \end{pmatrix} = \psi = \begin{pmatrix} \psi_1 \\ -X\psi_1^* \end{pmatrix}, \tag{14}$$

and as such the Dirac operator "preserves" X-conjugacy (because the corresponding real operator does not mix real and imaginary parts). Thus, to determine ψ we need only compute

$$\psi_1 = \mathcal{M}_{11}\chi_1 - \mathcal{M}_{12}X\chi_1^* \equiv \mathcal{M}_X\chi_1, \tag{15}$$

and reconstruct the lower component of ψ afterwards. In the above we have defined a new single-flavor "X-conjugate Dirac operator", $\mathcal{M}_X$; this is a somewhat odd construction as it does not act like a linear operator due to the complex conjugation. Nevertheless, as $\mathcal{M}_{11}$ connects only sites in the "bulk" (i.e. not across the boundary), and $\mathcal{M}_{12}$ – which induces the G-parity flavor mixing – exists only across the boundary, we can implement $\mathcal{M}_X$ as a regular, *single-flavor* Dirac operator but with "X-conjugate BCs": $\hat{T}\psi(L-1)\hat{T}^{-1} = -X\psi^*(0)$, and $\hat{T}^{-1}\psi(0)\hat{T} = X\psi^*(L-1)$ where $\hat{T}$ is the translation operator. These were straightforward to implement Grid. The implications of the non-linearity of this Dirac operator also turn out to be generally benign; for instance, the conjugate gradient acting on $\mathcal{M}_X^\dagger \mathcal{M}_X$ can be used in an unmodified form to compute the inverse.

5. Gauge evolution with the X-conjugate Dirac operator

The goal of this section is to demonstrate that the real, two-flavor pseudofermion integral in Eq. 11 can be rewritten in terms of a complex, single-flavor pseudofermion integral through the X-conjugate Dirac operator. Define $\xi = \mathcal{M}^{-1}\chi$, such that

$$-\chi^\dagger (\mathcal{M}\mathcal{M}^\dagger)^{-1}\chi = -\xi^\dagger\xi . \tag{16}$$

From the structure of X-conjugate vectors, it is straightforward to show that $\xi^\dagger\xi = 2\xi_1^\dagger\xi_1$. Applying Eqs. 14 and 15,

$$\chi = \mathcal{M}\xi = \begin{pmatrix} \mathcal{M}_X\xi_1 \\ -X[\mathcal{M}_X\xi_1]^* \end{pmatrix}, \tag{17}$$

from which we identify $\xi_1 = \mathcal{M}_X^{-1}\chi_1$. Inserting these results into Eq. 16 gives

$$-\chi^\dagger (\mathcal{M}\mathcal{M}^\dagger)^{-1}\chi = -2\chi_1^\dagger (\mathcal{M}_X\mathcal{M}_X^\dagger)^{-1}\chi_1 . \tag{18}$$

We can scale out the factor of two by defining the single-flavor pseudofermion field $\rho = \sqrt{2}\chi_1$.

We must also address the Jacobian transform between the two-flavor real field $[d\phi_r'] \equiv \prod_x d\phi_{r,1}'(x)d\phi_{r,2}'(x)$ and the one-flavor complex field $[d\rho_r][d\rho_i] \equiv \prod_x d\rho_r(x)d\rho_i(x)$. From Eq. 13 we have $\rho_r = -X\phi_{r,1}'$ and $\rho_i = \phi_{r,2}'$, hence

$$J = \begin{bmatrix} \frac{\partial\phi_{r,1}'}{\partial\rho_r} & \frac{\partial\phi_{r,1}'}{\partial\rho_i} \\ \frac{\partial\phi_{r,2}'}{\partial\rho_r} & \frac{\partial\phi_{r,2}'}{\partial\rho_i} \end{bmatrix} = \begin{bmatrix} X & 0 \\ 0 & -1 \end{bmatrix} = -\det X = -1 \tag{19}$$

As a result, up to a trivial sign,

$$\det(\mathcal{M}) = \int [d\rho_r][d\rho_i] \exp\left(-\rho^\dagger (\mathcal{M}_X\mathcal{M}_X^\dagger)^{-1}\rho\right) . \tag{20}$$

Thus we obtain the two-flavor determinant in terms of the X-conjugate Dirac operator.

Exploiting hidden symmetries to accelerate the lattice calculation of $K \to \pi\pi$ decays with G-parity boundary condititons
Christopher Kelly
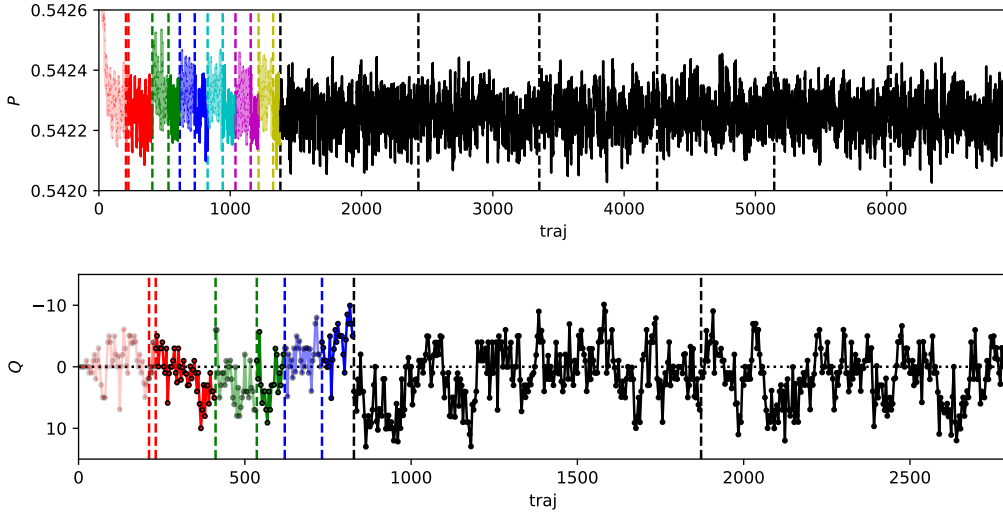
Figure 1: The evolution of the plaquette (upper) and topological charge (lower). Colored data indicate streams generated with the original action, and black with the new. For the former, lighter-shaded data are associated with thermalization and tuning; these regions are delineated by vertical lines of the corresponding color. For the new action, black vertical lines delineate the 6 streams of evolution. Here the topological charge has been measured only on a subset of the available trajectories.
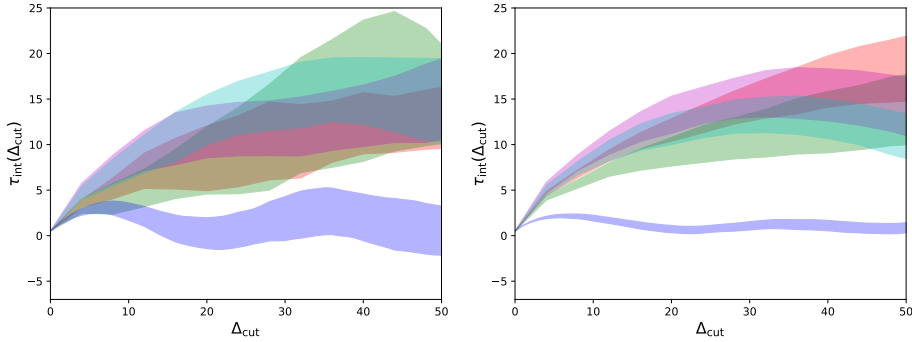
Figure 2: The measured integrated autocorrelation time $\tau_{\text{int}} = \frac{1}{2} + \sum_{t=1}^{\Delta_{\text{cut}}} C(t)$ for increasing Δ_{cut}, where $C(t)$ is the autocorrelation function. Data comprise the topological charge (red), its square (green), the plaquette (blue), and the Wilson flow scales w_0 (mauve) and $t_0^{1/2}$ (cyan). The left plot is for a single stream of the original action, and the right for the new action.

6. Application for production running

In order to address the discretization systematic error in our $K \to \pi\pi$ calculation, we are generating a new $40^3 \times 64$ Möbius domain wall fermion lattice with physical quark masses, $L_s = 12$, $b+c = 2$, using the Iwasaki+DSDR gauge action at $\beta = 1.848$, and G-parity BCs in three directions. This "40ID" ensemble has the same physical volume as our 2020 calculation in order to ensure the decay remains energy conserving, but has a finer $a^{-1} = 1.72$ GeV lattice spacing than the $a^{-1} = 1.38$ GeV of our previous work. The evolution is being performed on the NERSC Perlmutter computer, with our tuned, production evolution with the original G-parity Dirac operator requiring 4.36 hours on 32 nodes (139.5 node-hours) per trajectory. With the X-conjugate action we are now able to complete a trajectory in just 1.12 hours on 32 nodes (35.8 node hours), an almost 4× improvement in throughput. A more computationally efficient run – used for our production jobs – requires 1.61 hours on 16 nodes (25.8 node hours), a 5.4× reduction in resource cost per trajectory.

6

The largest gains resulted from the naïve 2× reduction in cost of applying the Dirac operator, coupled to no longer requiring the more-expensive EOFA action for the light quarks and RHMC action for the strange quarks; the light quarks now utilize the conventional squared-operator action, and we substitute the RHMC for the EOFA for the strange quarks now that we need compute only a square-root rather than a fourth-root of the determinant. The use of these cheaper actions also allowed for greater scope in tuning, enabling us to increase the number of Hasenbusch mass splittings [10] from 5 to 11 for the light quarks and from 1 to 3 for the strange quark. We also now employ the force-gradient [11, 12] rather than the Omelyan integrator, enabling us to run with larger outer step sizes of 0.125 molecular dynamics time units (MDTU) vs the 0.07 MDTU of our original runs, while retaining a high, 91% acceptance probability.

Running 6 parallel streams of evolution, we are very rapidly generating statistics. In Fig. 1 we plot the evolution of the plaquette to-date; clearly the volume of data generated with the new approach – around 5500 trajectories at the time of writing – now vastly eclipses the old. In the same figure we also plot the evolution of the topological charge for a subset of the data, showing good topological sampling. Finally, in Fig. 2 we plot the integrated autocorrelation times for the original and new actions; while the statistics are limited for the original action, we observe consistent $\tau_{\text{int}} \sim 15 - 20$ MDTU. Assuming we measure every 15th sample, we therefore have sufficient data to perform ~370 measurements, half way to matching the statistics of our 2020 calculation. At the present rate of generation we anticipate doubling this amount within 6 months.

7. Conclusions

Exploiting a symmetry of the two-flavor G-parity Dirac operator under complex conjugation, we have reformulated the two-flavor fermion determinant as a much cheaper integral of a conventional, single-flavor Dirac operator with "X-conjugate" BCs. With this approach we have achieved an almost 3× increase in ensemble generation speed and a 5.4× reduction in resource cost, for the production running of our new, finer "40ID" ensemble. In an upcoming publication we will also demonstrate how the X-conjugate approach can be used to speed up eigenvector generation and propagator inversion for the $K \to \pi\pi$ measurements by 2×. Together these breakthroughs vastly reduce the cost of measuring ϵ' with G-parity BCs.

References

[1] Z. Bai *et al.*, Phys. Rev. Lett. **115**, no.21, 212001 (2015) [arXiv:1505.07863 [hep-lat]].

[2] R. Abbott *et al.*, Phys. Rev. D **102**, no.5, 054509 (2020) [arXiv:2004.09440 [hep-lat]].

[3] T. Blum *et al.*, [arXiv:2306.06781 [hep-lat]].

[4] N. Christ *et al.*, Phys. Rev. D **106**, no.1, 014508 (2022) [arXiv:2111.04668 [hep-lat]].

[5] M. Tomii, PoS **LATTICE2019**, 174 (2020)

[6] N. H. Christ *et al.*, Phys. Rev. D **101**, no.1, 014506 (2020) [arXiv:1908.08640 [hep-lat]].

[7] Y. C. Chen *et al.*, Phys. Lett. B **738**, 55-60 (2014) [arXiv:1403.1683 [hep-lat]].

[8] C. Jung,*et al.*, Phys. Rev. D **97**, no.5, 054503 (2018) [arXiv:1706.05843 [hep-lat]].

[9] P. A. Boyle *et al.*, PoS **LATTICE2015**, 023 (2016)

[10] M. Hasenbusch, Phys. Lett. B **519**, 177-182 (2001) [arXiv:hep-lat/0107019 [hep-lat]].

[11] M. A. Clark *et al.*, Phys. Rev. D **84**, 071502 (2011) [arXiv:1108.1828 [hep-lat]].

[12] H. Yin *et al* PoS **LATTICE2011**, 051 (2011) [arXiv:1111.5059 [hep-lat]].